Bioconjugate Chemistry

Communication

pubs.acs.org/bc

Synthesis of Polymer–Lipid Nanoparticles for Image-Guided Delivery of Dual Modality Therapy

Aneta J. Mieszawska,[†] YongTae Kim,[‡] Anita Gianella,[†] Inge van Rooy,[†] Bram Priem,[†] Matthew P. Labarre,[§] Canturk Ozcan,[†] David P. Cormode,[∥] Artiom Petrov,[⊥] Robert Langer,[‡] Omid C. Farokhzad,[#] Zahi A. Fayad,[†] and Willem J. M. Mulder*[,†,¶]

[†]Translational and Molecular Imaging Institute and Imaging Science Laboratories and [⊥]Zena and Michael and Michael A. Wiener Cardiovascular Institute and Marie-Josée and Henry R. Kravis Center for Cardiovascular Health, Icahn School of Medicine at Mount Sinai, One Gustave L. Levy Place, New York, New York 10029, United States

[‡]David H. Koch Institute for Integrative Cancer Research, Department of Chemical Engineering and Division of Health Science and Technology, Massachusetts Institute of Technology, Cambridge, Massachusetts 02139, United States

[§]Department of Materials Science and Engineering, University of Pennsylvania, 3451 Walnut Street, Philadelphia, Pennsylvania 19104, United States

[∥]Radiology Department, University of Pennsylvania, 3400 Spruce Street, 1 Silverstein, Philadelphia, Pennsylvania 19104, United States

[#]Laboratory of Nanomedicine and Biomaterials, Department of Anesthesiology, Brigham & Women's Hospital, Harvard Medical School, 75 Francis Street, Boston, Massachusetts 02115, United States

[¶]Department of Vascular Medicine, Academic Medical Center, Amsterdam, The Netherlands

Supporting Information

ABSTRACT: For advanced treatment of diseases such as cancer, multicomponent, multifunctional nanoparticles hold great promise. In the current study we report the synthesis of a complex nanoparticle (NP) system with dual drug loading as well as diagnostic properties. To that aim we present a methodology where chemically modified poly(lactic-*co*-glycolic) acid (PLGA) polymer is formulated into a polymer–lipid NP that contains a cytotoxic drug doxorubicin (DOX) in the polymeric core and an anti-angiogenic drug sorafenib (SRF) in the lipidic corona. The NP core also contains gold nanocrystals (AuNCs) for imaging purposes and cyclodextrin molecules to maximize the DOX encapsulation in the NP core. In addition, a near-infrared (NIR) Cy7 dye was incorporated in the coating. To fabricate the NP we used a microfluidics-based technique that offers unique NP synthesis conditions, which allowed for encapsulation and fine-tuning of optimal ratios of all the NP components. NP phantoms could be visualized with computed tomography (CT) and near-infrared (NIR) fluorescence imaging. We observed timed release of the encapsulated drugs, with fast release of the corona drug SRF and delayed release of a core drug DOX. In tumor bearing mice intravenously administered NPs were found to accumulate at the tumor site by fluorescence imaging.

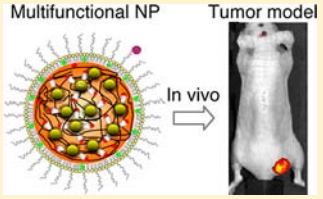

INTRODUCTION

Advances in nanotechnology in general, and nanoparticle (NP) production methods specifically, have facilitated and accelerated the development of complex multicomponent nanomaterials. In the past decade, a significant research effort by the nanomedicine community was focused on the development and preclinical application of NP platforms.[1−3] NP-drug formulations can solubilize or shield hydrophobic or highly toxic cytostatic agents and overcome bioavailability challenges.[4−6] Also, NP systems can be used to alter pharmacokinetics and increase the percentage of injected drug dose that accumulates at the diseased site.[7−9] Finally, their favorable size range and the ease of surface functionalization enable targeting of NPs to specific cell types at these diseased sites.[10,11] However, the assembly of multiple materials and/or agents into one NP formulation is challenging and frequently necessitates extreme synthetic conditions that by themselves can impair functionality of the individual NP components.

In the current report, we present a highly complex and multifunctional hybrid polymer–lipid NP platform that incorporates diagnostic nanocrystals and two therapeutic drugs. The complexity of the proposed NP required selecting a suitable synthesis method that would facilitate the integration of all functionalities into the NP, since other widely used NP synthesis techniques, including nanoprecipitation,[12] have failed to incorporate all necessary components into a NP. To this aim we used a two-pronged approach that involved chemical modification of a polymer and the use of microfluidic technology, that we recently developed for high-throughput

Received: April 2, 2013
Revised: June 17, 2013
Published: August 19, 2013

dx.doi.org/10.1021/bc400166j | *Bioconjugate Chem.* 2013, 24, 1429−1434

polymer NP synthesis.[13] This microfluidic system provides a controlled mixing environment, which facilitates NP assembly through microvortices[14] at ambient conditions.

The NP core is composed of a biodegradable poly(lactic-*co*-glycolic acid) (PLGA) polymer, functionalized with gold nanocrystals (AuNCs), which serve as scaffolds that are loaded with doxorubicin (DOX), a widely used cytostatic agent.[15,16] Since AuNCs are electron dense and exhibit good X-ray attenuation properties, the NP platform can be imaged by electron microscopy and computed tomography (CT).[17,18] The NP coating is composed of ordinary phospholipids and PEGylated phospholipids at a 7/3 ratio, which by themselves form stable disks.[19] The latter facilitates the formation of a lipid monolayer around the PLGA core. This lipid coating provides biocompatibility, while PEG reduces clearance by the mononuclear phagocyte system (MPS) and thereby elongates circulation half-lives.[20] We also used the lipidic coating to coencapsulate a second lipophilic drug sorafenib (SRF). SRF is an angiogenesis inhibitor with antitumor activity.[21] Lastly, the PEG coating was labeled with Cy7 fluorophores for near-infrared fluorescence (NIRF) imaging.

For cancer treatment the combination of administering an anti-angiogenic and cytotoxic agent holds great promise to maximize the therapeutic outcome by interfering with the tumor blood/nutrients supply and simultaneously inducing cancer cell apoptosis.[22−24] However, an impaired vascular system also reduces the cytostatic agent influx into the tumor. NP systems accumulate at tumorous sites with a leaky vasculature through the enhanced permeability and retention effect (EPR)[25] and increase drug bioavailability and prolong the exposure to therapeutic agents providing slow release.[26] Dual drug loading in the NP systems with controlled release rates would potentially address the described limitations of the aforementioned combined drug therapy.

RESULTS AND DISCUSSION

Previous PLGA-DOX formulations have already been explored.[27,28] Nevertheless, it remains challenging to incorporate high doses of DOX into the NP core. In order to overcome this issue, we chemically modified PLGA using esterification reaction sequentially, as shown in Scheme 1. First, 1−3 nm AuNCs were conjugated to the PLGA polymer and subsequently these AuNCs were derivatized with hydroxypropyl *β*-cyclodextrin (HP-*β*CD), a cyclic drug host molecule[29,30] that can be incorporated into polymeric NPs.[31] To that end the carboxyl groups of 11-mercaptoundecanoic acid (MUA) capped 3 nm AuNCs were reacted with hydroxyl groups of PLGA monomers using *N,N′*-dicyclohexylcarbodiimide (DCC) and 4-dimethylaminopyridine (DMAP), which resulted in the formation of an ester bond between the ligands of AuNCs and PLGA monomers. The same reaction conditions were used to attach HP-*β*CD to the AuNCs. To maximize loading of AuNCs and HP-*β*CD to the PLGA polymer, the esterification reaction can be repeated multiple times, to create AuNC:HP-*β*CD:AuNC:HP-*β*CD:etc. chains. ^{1}H NMR was performed after each esterification step to confirm successful modification of the PLGA polymer (Figure S1, Supporting Information). From the ^{1}H NMR analyses it was found that there were 3.44 HP-*β*CD molecules per PLGA monomer. In addition, the yield for each step of the PLGA modification was quantified. The Au concentration derived from CT measurements, for which detailed calculations are presented in the Supporting Information, was found to be 0.7 mg Au/100 mg of PLGA (89% of the initial input value) and the concentration of HP*β*CDs derived from NMR was established to be 12 mg HP*β*CDs/100 mg PLGA (24% of the initial input value).

Scheme 1. Modification of a PLGA Polymer with AuNCs and HP-*β*CDs via an Esterification Reaction and Subsequent Host−Guest Inclusion of DOX in HP-*β*CDs[a]

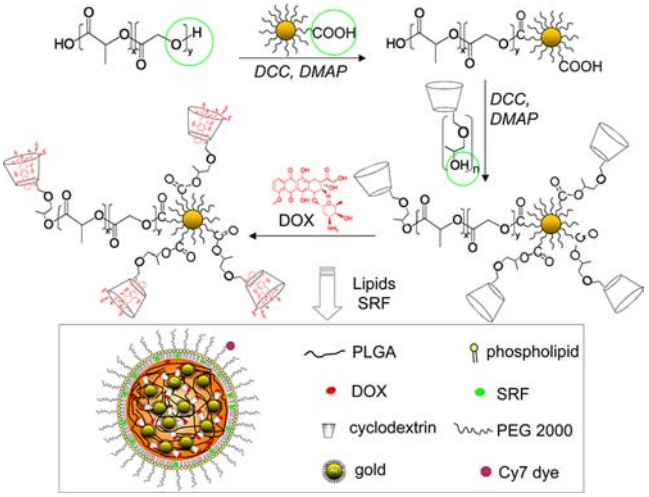

[a]Boxed: Lipid-polymer NP formed from modified PLGA, lipids, and SRF.

The modified PLGA-AuNCs-HP-*β*CD was incubated with DOX prior to NP synthesis to ensure DOX-HP*β*CD complex formation. The microfluidic chip for the rapid polymer−lipid NP synthesis[13] is shown in Figure 1A. PLGA modified with AuNCs-HP-*β*CDs-DOX in acetonitrile was infused in the center channel of a microfluidic chip. PEGylated phospholipids (PEG-DSPE) and 1,2-dipalmitoyl-*sn*-glycero-3-phosphocholine (DPPC) in a 7:3 ratio were combined with SRF in 30% methanol in water and infused in the external channels. 0.3 mol % of PEG-DSPE labeled with the NIRF Cy7 dye was added to the lipids.

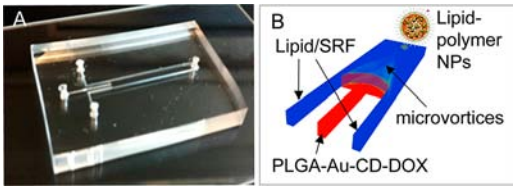

Figure 1. (A) Microfluidic chip and (B) schematic of the flow pattern in the microfluidic chip.

The polymer−lipid NPs were assembled by dual microvortices created at the intersection of the three inlets of the microfluidic chip (Figure 1B) at a flow rate of 5 mL/min in the external channels and 1 mL/min in the center channel, which corresponded to a Reynolds number[32] of 150. These conditions provide controlled mixing environment on the microscale and facilitate the swift assembly of uniform NPs, as explained in detail previously.[13] The DOX loading, established by HPLC, was 25.6% of the initial input value. This value is 19 times higher than DOX loading in polymer−lipid NPs where PLGA was not modified with HP-*β*CDs (1.3% of the initial input value). Our strategy resulted in 2 (molar %) times higher DOX encapsulation in PLGA NPs as compared to a previously published method where DOX was directly conjugated to the

dx.doi.org/10.1021/bc400166j | *Bioconjugate Chem.* 2013, 24, 1429−1434

PLGA polymer to elevate its encapsulation into the NP core and the NPs were formed using an emulsion−solvent diffusion method.[28] The SRF encapsulation efficiency was established to be 66.0% of the initial input value.

The engineered polymer−lipid NPs were thoroughly characterized with respect to efficiency of AuNCs encapsulation, size, and contrast generating properties, as depicted in Figure 2. Transmission electron microscopy (TEM) revealed

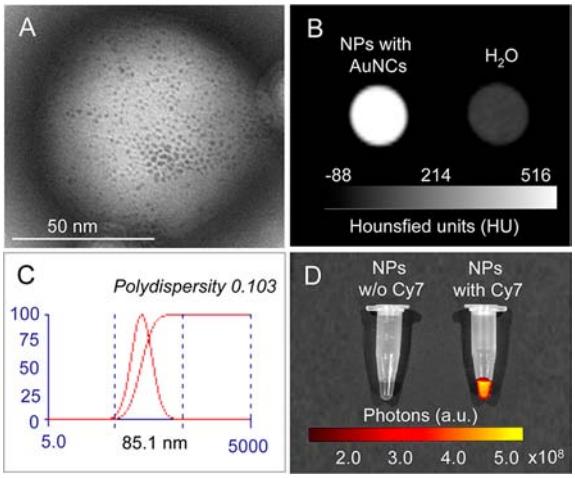

Figure 2. (A) TEM image of a single engineered lipid−polymer NP revealing encapsulated AuNCs; (B) CT image of phantoms containing AuNC loaded lipid−polymer NPs or water; (C) DLS measurements of the NP platform; (D) fluorescence from Cy7 dye conjugated to NP's lipid corona.

the uniform incorporation of AuNCs in polymer−lipid NPs (Figure 2A, enlarged image Figure S2). The NPs generated CT contrast, as shown in Figure 2B, and the CT attenuation rate[33] was 5.23 HU/mM as established previously.[34] The mean overall diameter of polymer−lipid NPs was 85.1 nm with a polydyspersity of 0.1 as measured by dynamic light scattering (DLS) (Figure 2C). Importantly, due to the Cy7 incorporated in the lipid corona, the NPs produced strong fluorescence in the NIR region as shown in Figure 2D.

We tested the polymer−lipid NPs for drug release under physiological conditions (in PBS at 37 °C), the results of which are shown in Figure 3. Drug concentrations were quantified using HPLC (see Supporting Information for experimental details, Figure S3 and S4). The SRF onset release was observed after 1 h, and DOX after 5 h. The delayed release of DOX corroborates that the drug is incorporated in the polymeric core while the rapid release of SRF indicates its incorporation within

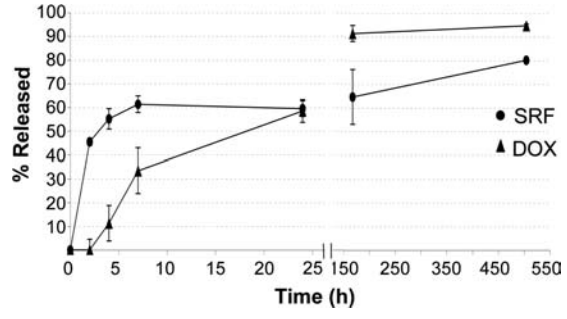

Figure 3. Release profiles of SRF and DOX from NPs in PBS at 37 °C.

the lipid corona of the NP. The rigidity of the lipidic coating, which has a phase transition temperature well above 37 °C, contributes to the partial preservation of SRF and its prolonged release. Both SRF and DOX continued to be released from the NPs for 21 days, classifying this nanoparticle as a second generation sustained release platform.

To test biological activity human umbilical vein cells (HUVECs) and a human colon cancer cell line (LS174T) were incubated with NPs and cell viability was measured (Figure 4A). NPs containing both SRF and DOX reduced cell

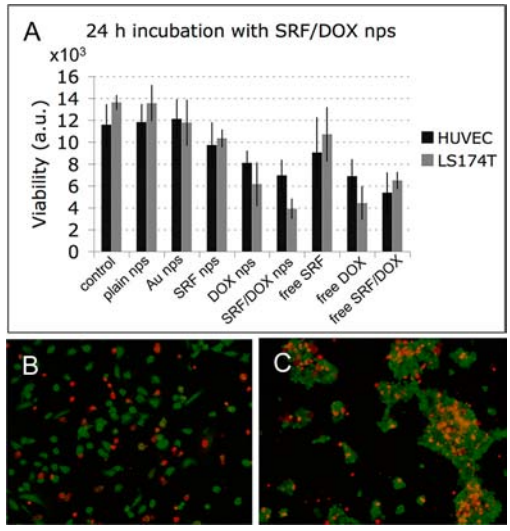

Figure 4. In vitro viability assays after incubating HUVEC and LS174T cells for 24 h with lipid−polymer NPs containing SRF and DOX. (A) Luminescent cell viability assay; (B) Live (green)/dead (red) staining of HUVEC; (C) Live/dead staining of LS 174T cells.

viability of HUVECs by 42% and the cell viability of LS174T cells by 72% as compared to the untreated control groups after 24 h of incubation. Cell viability was less affected by NPs containing a single drug, while the viability of cells incubated with NPs without a drug were similar to the untreated cells. We confirmed the results by live/dead staining (Figure 4B and C). After 24 h incubation, the number of dead cells was negligible for untreated cells as well as for cells treated with plain NP or NP containing AuNCs only. The number of dead cells increased for single drug NP formulations (see Supporting Information Figure S5 for the control experiments). The concurrent presence of SRF and DOX in the NP formulation maximized the cytotoxic effects for both HUVECs and LS174T cells (Figure 4B−C). The release profiles (fast SRF and delayed DOX release) combined with the in vitro finding suggest that our NP platform may indeed find use as a NP that accumulates at the tumor site, acts on existing tumor blood vessels, and prevents angiogenesis by SRF, followed by DOX-induced cancer cell death. However, extensive mouse studies are required to establish the efficacy of our NPs in vivo in future studies.

However, we did perform pilot in vivo studies with tumor bearing mice to evaluate the NP tumor targeting potential. The NPs were intravenously administered into tumor bearing mice (n = 3) and the animals were imaged 18 h post injection. Blood samples were collected at various time points. Optical measurements and fitting of the data revealed the in vivo half-life of NPs to be 40 min. Anatomical CT imaging revealed

dx.doi.org/10.1021/bc400166j | Bioconjugate Chem. 2013, 24, 1429−1434

the presence of a tumor on the flank of the animals. Figure 5A depicts a reconstructed 3D CT image of mouse topography;

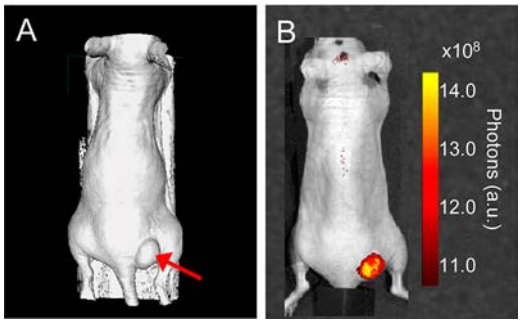

Figure 5. In vivo imaging of NPs biodistribution. (A) Reconstructed CT image of a tumor bearing mouse (arrow indicates the tumor), (B) NIRF imaging of strong Cy7 fluorescence in the tumor, indicative of NP accumulation.

the arrow indicates the tumor site. Although the NPs contained gold tumor accumulation did not result in a detectable CT signal attenuation. Among the different imaging modalities CT is relatively insensitive to detecting exogenous agents. Although the AuNCs can also serve as a CT contrast agent,[8] the AuNCs in the presented lipid–polymer NP primarily serve as inert scaffolds[35,36] and their payload can potentially be increased as shown previously,[34] providing the option to use this NP platform as a CT imaging tool as well. However, NIRF imaging, a very sensitive imaging modality, revealed the accumulation of NPs in tumors (Figure 5B). Due to the limited imaging depth of NIRF imaging we also performed ex vivo NIRF of excised organs to more accurately establish NP biodistribution in relevant organs (Supporting Information Figure S6). Finally, to corroborate the accumulation of NPs we performed the immunofluorescence of tumor sections, depicted in Figure 6. Staining of endothelial cells (red) indicates tumor blood vessels. NPs (green) were found in close proximity of the vessels (Figure 6A) as well as in tumor interstitium (Figure 6B) indicative of NP extravasation and tumor accumulation.

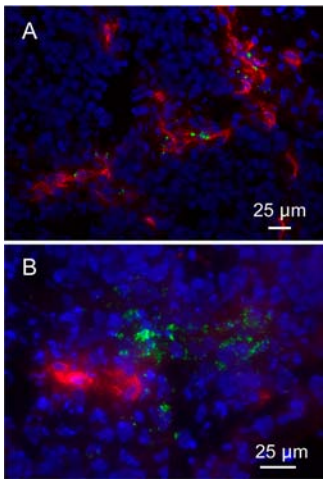

Figure 6. Immunofluorescence of tumor sections. CD31 staining shows endothelial cells in red, the NPs are shown in green, and the nuclei are stained with DAPI in blue. (A) The NPs were found associated with tumor blood vessels as well as (B) accumulated in the tumor interstitium.

Ongoing studies are aimed to further optimize the NP's physicochemical properties as well as AuNCs payload per NP to enhance the NP tumor accumulation, and improve the in vivo NP detection by CT, respectively.

CONCLUSION

In summary, we combined simple carbodiimide conjugation chemistry to modify the PLGA polymer to synthesize a complex and multifunctional theranostic polymer–lipid NP platform with microfluidic technology. Two drugs, i.e., the antiangiogenic drug SRF and cytotoxic drug DOX, for combined cancer therapy were successfully encapsulated in the lipid corona and polymeric core, respectively. Release profiles showed a quick release of SRF and a delayed release of DOX. Finally, an in vivo pilot NIRF imaging experiment revealed the accumulation of the NPs at the tumor site, and immunofluorescence of tumor sections revealed distribution of the NPs within the tumor space. Future studies are planned to evaluate the efficacy of our approach in vivo in tumor bearing mice. In addition to cancer therapy the flexibility of our NP platform allows for incorporation of other therapeutics and applications of a theranostic NP probe for atherosclerotic disease or other pathologies that are characterized by ongoing angiogenesis.

EXPERIMENTAL SECTION

Materials. 1-dodecanethiol, 11-mercaptoundecanoic acid, 4-dimethylaminopyridine, *N,N′*-dicyclohexylurea, Poly(D,L-lactide-*co*-glycolide) lactide:glycolide (50:50), mol wt 30,000–60,000, chloroauric acid, sodium borohydride, methyl trioctylammonium chloride, cis-9-octadecene-1-thiol, (2-Hydroxypropyl)-*β*-cyclodextrin, and doxorubicin hydrochloride were purchased from Sigma-Aldrich (St. Louis, MO). 1,2-Distearoyl-*sn*-glycero-3-phosphoethanolamine-*N*-[methoxy(polyethylene glycol)-2000] (PEG2000-DSPE) and 1,2-dipalmitoyl-*sn*-glycero-3-phosphocholine (DPPC) were purchased from Avanti Polar Lipids, Inc. (Alabaster, AL). Sorafenib *p*-toluenesulfonate salt was purchased from Biotang Inc. (Lexington, MA).

Synthesis of Au Nanocrystals (AuNCs). AuNCs coated with 1-dodecanethiol were prepared using a previously published method by Brust et al.[37] The AuNCs were 1–3 nm in diameter and the hydrophobic nature of the capping ligands rendered them soluble in organic solvents such as toluene and chloroform.

AuNCs Ligand Exchange. Hydrophobic dodecanethiol ligands on AuNCs (108 ligands per one AuNC) were exchanged to mercaptoundecanoic acid (MUA) following the Murray method.[38] 100 mg of dodecanethiol capped AuNCs were dissolved in 20 mL of toluene and mixed with 70 mg of MUA (at a 1:5 molar ratio of dodecanethiol:MUA) and stirred for 96 h. Next, toluene was removed by evaporation using a rotary evaporator with a 70 °C water bath. The AuNCs were resuspended and washed with acetonitrile (ACN) and collected on a frit (Opti Chem). The ligand exchange reaction renders the AuNCs-MUA soluble in polar solvents, i.e., ethanol (EtOH), methanol (MeOH), or dimethylformamide (DMF).

PLGA Modification with AuNCs and (2-Hydroxypropyl)-*β*-cyclodextrin (HP-*β*CD). 100 mg of PLGA (average MW of 60,000 g/mol) and 3 mg of AuNCs-MUA (centrifuged at 14.5K rpm to remove precipitated AuNCs) were dissolved in 1 mL of DMF. The esterification reaction between the alcohol group of PLGA and the carboxylic acid group of MUA was

performed using the coupling reagent *N,N′*-dicyclohexylurea (DCC), and the base 4-dimethylaminopyridine (DMAP), which were added at 20 mM concentration (both). After 3 h of gentle stirring, DMF was evaporated and PLGA-AuNC conjugates were dissolved in ACN at a concentration of 20 mg/mL and stored overnight in −20 °C freezer to precipitate unreacted AuNCs. The supernatant was used in further steps. Next, the PLGA-AuNCs were transferred to 1 mL DMF, mixed with 50 mg of HP-βCD (5× molar excess with respect to PLGA) and 20 mM DCC and DMAP and stirred for 3 h. After 3 h DMF was evaporated and PLGA-AuNCs-HP-βCD dissolved in ACN at a concentration of 20 mg/mL of PLGA, stored in −20 °C freezer overnight to precipitate unreacted HP-βCD. The supernatant was used in subsequent steps. The coupling of AuNCs to PLGA-AuNCs-HP-βCD was repeated. The final PLGA-AuNCs-HP-βCD-AuNCs solution in ACN was clear and tinted brownish/red. Small fraction of the PLGA polymer was modified with Cy5.5 using the same conjugation chemistry.

Formation of Lipid−Polymer NPs Using Microfluidics. Lipid−polymer NPs were formed using a microfluidic method developed by Kim et al.[13] In short, 250 μg of doxorubicin was dissolved in DMF and mixed with 12 mg of PLGA-AuNCs-HP-βCD-AuNCs in ACN at 2 mg/mL final PLGA concentration. 250 μg of sorafenib (SRF) was mixed with 59.5 mL of DPPC/DSPE-PEG (molar ratio of 3:7 of DPPC:DSPE-PEG and 0.3 molar % of DSPE-PEG-Cy7) in 30% MeOH/H_2O at 0.04 mg/mL of total lipids. The PLGA-AuNCs-HP-βCD-DOX-AuNCs solution was infused in the middle channel at 1 mL/min and lipids-SRF solution in the external channels at 5 mL/min. The formed lipid−polymer NP solution was stirred overnight under the fume hood to evaporate the solvents, subsequently filtered through a 0.22 μm syringe filter to remove the residual DCC and washed extensively with water using Vivaflow 50 filtration system (Sartorius, Bohemia, NY) to remove residual DMAP and unbound DOX/SRF. The NPs used in fluorescent imaging of tumor sections contained 7 mol % of PLGA labeled with Cy5.5.

In Vitro Drug Release Experiments. The NPs were washed thoroughly with purified water after the synthesis and preconcentrated using a Vivaflow 50 filtration system (Sartorius, Bohemia, NY). 500 μL of NP samples, corresponding to 4 mg of PLGA each, were placed in dialysis cassettes with a 2 kDa MWCO membrane (Pierce, Rockford, IL). At each time point three NP samples were collected, dried under vacuum, and the drugs were resolubilized in 500 μL of methanol. The samples were then centrifuged at 14.5K rpm for 5 min to remove the polymer and the supernatant was collected. The samples were analyzed for SRF and DOX content using HPLC as described in Supporting Information.

Tumor Mouse Model. To establish subcutaneous tumors 4 female nude mice were inoculated with 2×10^6 LS174T cells on the right flank. After 4 days the tumors were palpable and at 9 days tumor volumes reached 100−120 mm^3. NPs corresponding to 240 mg of PLGA and labeled with the near-infrared dye Cy7 were administrated trough tail vein injection to 3 mice. One mouse was not injected and was used as a control. Eighteen hours post injection, mice were anesthetized using ketamine/xylamine mixture (100 mg/kg/10 mg/kg) to enable in vivo CT and near-infrared fluoresce (NIRF) imaging. After in vivo imaging mice were sacrificed and the organs collected for NIRF imaging of NP biodistribution. For the in vivo half-life the blood samples were drawn from the lateral saphenous vein at 5, 10, 60, and 120 min after injection.

Immunofluorescence. Frozen tumor sections were prepared using a cryostat. Standard immunostaining techniques were appled for CD31 and DAPI. In short, the sections were blocked with donkey serum for 20 min, washed with PBS, and incubated with rat anti-mouse CD31 antibody (BD Pharmigen #553370) for 45 min. The slides were rinsed with PBS and incubated with secondary donkey anti-rat antibody (Jackson Immuno Research Laboratories, Inc. #712−165−150) labeled with Cy3 for 30 min, rinsed with PBS, and mounted in mounting medium with DAPI (Vector laboratories, Burlingame CA). The stained tumor sections were imaged using Leica Microsystems DM6000 microscope controlled using Leica Application Suite Advanced Fluorescence (LAS AF) software version 3.1.0 build 8587. The microscope was fitted with a Leica DFC350 FX camera. Sections were imaged at 40 and 63 times magnification.

■ ASSOCIATED CONTENT

Ⓢ Supporting Information

Description of characterization methods; ^{1}H NMR spectra; TEM image of NPs; HPLC calibration curves and spectra of SRF and DOX; NIRF images of organs. This material is available free of charge via the Internet at http://pubs.acs.org.

■ AUTHOR INFORMATION

Corresponding Author

*E-mail: willem.mulder@mssm.edu.

Notes

The authors declare no competing financial interest.

■ ACKNOWLEDGMENTS

This work was supported by the National Heart, Lung, and Blood Institute, National Institutes of Health, as a Program of Excellence in Nanotechnology (PEN) Award, Contract #HHSN268201000045C, as well as by R01 EB009638 (Z.A.F.), R00 EB012165 (D.P.C.) and R01 CA155432 (W.J.M.M.).

■ REFERENCES

(1) Peer, D., Karp, J. M., Hong, S., Farokhzad, O. C., Margalit, R., and Langer, R. (2007) Nanocarriers as an emerging platform for cancer therapy. *Nat. Nanotechnol. 2*, 751−60.

(2) Torchilin, V. P. (2005) Recent advances with liposomes as pharmaceutical carriers. *Nat. Rev. Drug Discovery 4*, 145−60.

(3) Wagner, V., Dullaart, A., Bock, A. K., and Zweck, A. (2006) The emerging nanomedicine landscape. *Nat. Biotechnol. 24*, 1211−7.

(4) Dalwadi, G., and Sunderland, B. (2009) An ion pairing approach to increase the loading of hydrophilic and lipophilic drugs into PEGylated PLGA nanoparticles. *Eur. J. Pharm. Biopharm. 71*, 231−42.

(5) Wischke, C., and Schwendeman, S. P. (2008) Principles of encapsulating hydrophobic drugs in PLA/PLGA microparticles. *Int. J. Pharm. 364*, 298−327.

(6) Zhang, L., Chan, J. M., Gu, F. X., Rhee, J. W., Wang, A. Z., Radovic-Moreno, A. F., Alexis, F., Langer, R., and Farokhzad, O. C. (2008) Self-assembled lipid–polymer hybrid nanoparticles: a robust drug delivery platform. *ACS Nano 2*, 1696−702.

(7) Avgoustakis, K., Beletsi, A., Panagi, Z., Klepetsanis, P., Karydas, A. G., and Ithakissios, D. S. (2002) PLGA-mPEG nanoparticles of cisplatin: in vitro nanoparticle degradation, in vitro drug release and in vivo drug residence in blood properties. *J. Controlled Release 79*, 123−35.

(8) Cormode, D. P., Roessl, E., Thran, A., Skajaa, T., Gordon, R. E., Schlomka, J. P., Fuster, V., Fisher, E. A., Mulder, W. J., Proksa, R., and Fayad, Z. A. (2010) Atherosclerotic plaque composition: analysis with multicolor CT and targeted gold nanoparticles. *Radiology 256*, 774−82.
(9) Gianella, A., Jarzyna, P. A., Mani, V., Ramachandran, S., Calcagno, C., Tang, J., Kann, B., Dijk, W. J., Thijssen, V. L., Griffioen, A. W., Storm, G., Fayad, Z. A., and Mulder, W. J. (2011) Multifunctional nanoemulsion platform for imaging guided therapy evaluated in experimental cancer. *ACS Nano 5*, 4422−33.
(10) Hrkach, J., Von Hoff, D., Mukkaram Ali, M., Andrianova, E., Auer, J., Campbell, T., De Witt, D., Figa, M., Figueiredo, M., Horhota, A., Low, S., McDonnell, K., Peeke, E., Retnarajan, B., Sabnis, A., Schnipper, E., Song, J. J., Song, Y. H., Summa, J., Tompsett, D., Troiano, G., Van Geen Hoven, T., Wright, J., LoRusso, P., Kantoff, P. W., Bander, N. H., Sweeney, C., Farokhzad, O. C., Langer, R., and Zale, S. (2012) Preclinical development and clinical translation of a PSMA-targeted docetaxel nanoparticle with a differentiated pharmacological profile. *Sci. Transl. Med. 4*, 128ra39.
(11) Sengupta, S., Eavarone, D., Capila, I., Zhao, G., Watson, N., Kiziltepe, T., and Sasisekharan, R. (2005) Temporal targeting of tumour cells and neovasculature with a nanoscale delivery system. *Nature 436*, 568−72.
(12) Xiong, S., Zhao, X., Heng, B. C., Ng, K. W., and Loo, J. S. (2011) Cellular uptake of Poly-(D,L-lactide-co-glycolide) (PLGA) nanoparticles synthesized through solvent emulsion evaporation and nanoprecipitation method. *Biotechnol. J. 6*, 501−8.
(13) Kim, Y., Lee Chung, B., Ma, M., Mulder, W. J., Fayad, Z. A., Farokhzad, O. C., and Langer, R. (2012) Mass production and size control of lipid-polymer hybrid nanoparticles through controlled microvortices. *Nano Lett. 12*, 3587−91.
(14) Marre, S., and Jensen, K. F. (2010) Synthesis of micro and nanostructures in microfluidic systems. *Chem. Soc. Rev. 39*, 1183−202.
(15) Duyndam, M. C., van Berkel, M. P., Dorsman, J. C., Rockx, D. A., Pinedo, H. M., and Boven, E. (2007) Cisplatin and doxorubicin repress Vascular Endothelial Growth Factor expression and differentially down-regulate Hypoxia-inducible Factor I activity in human ovarian cancer cells. *Biochem. Pharmacol. 74*, 191−201.
(16) Fornari, F. A., Randolph, J. K., Yalowich, J. C., Ritke, M. K., and Gewirtz, D. A. (1994) Interference by doxorubicin with DNA unwinding in MCF-7 breast tumor cells. *Mol. Pharmacol. 45*, 649−56.
(17) Hainfeld, J. F., Slatkin, D. N., Focella, T. M., and Smilowitz, H. M. (2006) Gold nanoparticles: a new X-ray contrast agent. *Br. J. Radiol. 79*, 248−53.
(18) Xu, C., Tung, G. A., and Sun, S. (2008) Size and concentration effect of gold nanoparticles on X-ray attenuation as measured on computed tomography. *Chem. Mater. 20*, 4167−4169.
(19) Johnsson, M., and Edwards, K. (2003) Liposomes, disks, and spherical micelles: aggregate structure in mixtures of gel phase phosphatidylcholines and poly(ethylene glycol)-phospholipids. *Biophys. J. 85*, 3839−47.
(20) Gref, R., Minamitake, Y., Peracchia, M. T., Trubetskoy, V., Torchilin, V., and Langer, R. (1994) Biodegradable long-circulating polymeric nanospheres. *Science 263*, 1600−3.
(21) Wilhelm, S. M., Adnane, L., Newell, P., Villanueva, A., Llovet, J. M., and Lynch, M. (2008) Preclinical overview of sorafenib, a multikinase inhibitor that targets both Raf and VEGF and PDGF receptor tyrosine kinase signaling. *Mol. Cancer Ther. 7*, 3129−40.
(22) Kerbel, R. S., and Kamen, B. A. (2004) The anti-angiogenic basis of metronomic chemotherapy. *Nat. Rev. Cancer 4*, 423−36.
(23) Ma, J., and Waxman, D. J. (2008) Combination of antiangiogenesis with chemotherapy for more effective cancer treatment. *Mol. Cancer Ther. 7*, 3670−84.
(24) Teoh, D., and Secord, A. A. (2012) Antiangiogenic agents in combination with chemotherapy for the treatment of epithelial ovarian cancer. *Int. J. Gynecol. Cancer 22*, 348−59.
(25) Iyer, A. K., Khaled, G., Fang, J., and Maeda, H. (2006) Exploiting the enhanced permeability and retention effect for tumor targeting. *Drug Discovery Today 11*, 812−8.
(26) Mattheolabakis, G., Rigas, B., and Constantinides, P. P. (2012) Nanodelivery strategies in cancer chemotherapy: biological rationale and pharmaceutical perspectives. *Nanomedicine 7*, 1577−90.
(27) Jia, Y., Yuan, M., Yuan, H., Huang, X., Sui, X., Cui, X., Tang, F., Peng, J., Chen, J., Lu, S., Xu, W., Zhang, L., and Guo, Q. (2012) Co-encapsulation of magnetic Fe3O4 nanoparticles and doxorubicin into biodegradable PLGA nanocarriers for intratumoral drug delivery. *Int. J. Nanomed. 7*, 1697−708.
(28) Yoo, H. S., Oh, J. E., Lee, K. H., and Park, T. G. (1999) Biodegradable nanoparticles containing doxorubicin-PLGA conjugate for sustained release. *Pharm. Res. 16*, 1114−8.
(29) Stella, V. J., and Rajewski, R. A. (1997) Cyclodextrins: their future in drug formulation and delivery. *Pharm. Res. 14*, 556−67.
(30) Uekama, K., Hirayama, F., and Irie, T. (1998) Cyclodextrin drug carrier systems. *Chem. Rev. 98*, 2045−2076.
(31) Tao, H. Q., Meng, Q., Li, M. H., Yu, H., Liu, M. F., Du, D., Sun, S. L., Yang, H. C., Wang, Y. M., Ye, W., Yang, L. Z., Zhu, D. L., Jiang, C. L., and Peng, H. S. (2013) HP-beta-CD-PLGA nanoparticles improve the penetration and bioavailability of puerarin and enhance the therapeutic effects on brain ischemia-reperfusion injury in rats. *Naunyn Schmiedebergs Arch. Pharmacol. 386*, 61−70.
(32) Nguyen, N. T., and Wu, Z. (2005) Micromixers-a review. *J. Micromech. Microeng. 15*, R1.
(33) Galper, M. W., Saung, M. T., Fuster, V., Roessl, E., Thran, A., Proksa, R., Fayad, Z. A., and Cormode, D. P. (2012) Effect of computed tomography scanning parameters on gold nanoparticle and iodine contrast. *Invest. Radiol. 47*, 475−81.
(34) Mieszawska, A. J., Gianella, A., Cormode, D. P., Zhao, Y., Meijerink, A., Langer, R., Farokhzad, O. C., Fayad, Z. A., and Mulder, W. J. (2012) Engineering of lipid-coated PLGA nanoparticles with a tunable payload of diagnostically active nanocrystals for medical imaging. *Chem. Commun. 48*, 5835−7.
(35) McMahon, K. M., Mutharasan, R. K., Tripathy, S., Veliceasa, D., Bobeica, M., Shumaker, D. K., Luthi, A. J., Helfand, B. T., Ardehali, H., Mirkin, C. A., Volpert, O., and Thaxton, C. S. (2011) Biomimetic high density lipoprotein nanoparticles for nucleic acid delivery. *Nano Lett. 11*, 1208−14.
(36) Zheng, D., Giljohann, D. A., Chen, D. L., Massich, M. D., Wang, X. Q., Iordanov, H., Mirkin, C. A., and Paller, A. S. (2012) Topical delivery of siRNA-based spherical nucleic acid nanoparticle conjugates for gene regulation. *Proc. Natl. Acad. Sci. U. S. A. 109*, 11975−80.
(37) Brust, M., Walker, M., Bethell, D., Schiffrin, D. J., and Whyman, R. (1994) Synthesis of thiol-derivatised gold nanoparticles in a two-phase Liquid-Liquid system. *J. Chem. Soc., Chem. Commun. 7*, 801−802.
(38) Guo, R., Song, Y., Wang, G., and Murray, R. W. (2005) Does core size matter in the kinetics of ligand exchanges of monolayer-protected Au clusters? *J. Am. Chem. Soc. 127*, 2752−7.